

# **Evaluation of Preliminary Models of the Geopotential in the United States**

**D. A. Smith and D. G. Milbert**

National Geodetic Survey, NOAA, SSMC3, 1315 East-West Hwy., Silver Spring, MD 20910

## **Introduction**

As members of the Special Working Group of the International Geoid Service, we have evaluated the preliminary geopotential models X01 through X05; computed by the joint NASA-GSFC/DMA project (Rapp and Nerem 1994). Our focus has been the behavior of these models in the conterminous United States. In this effort, our strategy has been to compare geoid models derived from geopotential coefficients against GPS ellipsoid heights located on optically-leveled benchmarks. This comparison is done in two ways. In one approach, the GPS benchmarks are compared against the geoid values obtained from what is essentially direct evaluation of the preliminary models. This approach suffers from the omission or truncation error inherent in an  $n=360$  model computation. In the other approach, the point gravity and digital terrain in and around the United States are used to compute high resolution geoid models in remove, compute, and restore procedures about the various preliminary models. While this approach alleviates the omission error problem, it is seen to remove portions of the geopotential model commission error.

In this report, we begin by outlining a few important points in the computation of gravimetric quantities from geopotential coefficients. Next, we review the features of the GPS benchmark data set that was used in evaluation of the preliminary models. We discuss the computation procedure used to obtain the high resolution geoid models, and display results with the GPS benchmark comparison. Then, we compare the geopotential models directly against the GPS benchmarks, without the removal of omission error. We close the report with conclusions and recommendations.

## **Geoid Height Computation**

It stands to reason that if one chooses to evaluate geopotential coefficients by means of GPS on leveled benchmarks, then one must use the utmost rigor in computation of the geoid heights from the coefficients. Towards this goal, we have developed formulations to support the use of geopotential coefficients computed with an arbitrary set of normal ellipsoid constants, and to support the computation of various gravimetric quantities relative to a different, arbitrary set of normal ellipsoid constants (which we take as GRS80). In addition, it must be recognized that the theory used to establish the geopotential coefficients is rooted in a solution of Laplace's equation. However, Laplace's equation only holds in a vacuum. The geoid over land is typically interior to the Earth's topography, where Poisson's equation would operate.

We begin by considering the evaluation of gravimetric quantities from spherical harmonic coefficients with arbitrary values of  $GM$  and  $a$ . The total external gravitational potential of the Earth can be expressed as:

$$V_1(r,\theta,\lambda) = \frac{GM_1}{r} \sum_{n=0}^{\infty} \left( \frac{a_1}{r} \right)^n \sum_{m=-n}^n \bar{C}_{nm} \bar{Y}_{nm}(\theta,\lambda)$$

where:

$r,\theta,\lambda$  = geocentric radial distance, colatitude, longitude

$GM_1, a_1$  = scale factors associated with the  $C_{nm}$  values

$\bar{C}_{nm}$  = fully normalized coefficients of the total field

$\bar{Y}_{nm}$  = fully normalized Legendre functions

And, the normal external gravitational potential of the Earth can be expressed as:

$$V_2(r,\theta,\lambda) = \frac{GM_2}{r} \sum_{n=0}^{\infty} \left( \frac{a_2}{r} \right)^n \sum_{m=-n}^n \bar{D}_{nm} \bar{Y}_{nm}(\theta,\lambda)$$

where:

$GM_2$  = Gravitation-Mass constant of the normal field

$a_2$  = semi-major axis of the ellipsoid and which is, of itself, a "spheropotential" surface, with constant value of normal gravity potential,  $U_0$ .

$\bar{D}_{nm}$  = fully normalized coefficients of the normal field  
(=0 if  $n$  is not positive even, or  $m$  is not zero)

The total external gravity potential of the Earth is:

$$W(r,\theta,\lambda) = V_1(r,\theta,\lambda) + \Phi(r,\theta)$$

and the normal external gravity potential of the Earth is:

$$U(r,\theta,\lambda) = V_2(r,\theta,\lambda) + \Phi(r,\theta)$$

where  $\Phi(r,\theta)$  is the centrifugal potential.

We make the following assumptions:

1)  $r,\theta,\lambda$  are the same in both equations, that is, the origins of the two fields coincide, as do their three Cartesian co-ordinate axes.

2) the value of normal gravity potential on the ellipsoid ( $U_0$ ), is equivalent, numerically, to the value of total gravity potential on the geoid ( $W_0$ )

3) The total and normal centrifugal potentials are equivalent, thus the disturbing potential, will be:  $T = W - U = V_1 - V_2$

Upon evaluating the disturbing potential, we pay careful attention to the differing values of  $GM_1$  versus  $GM_2$  and  $a_1$  versus  $a_2$ . We start by rewriting the equation for  $V_1$  as (and truncating the series at the given high value of 360):

$$V_1(r, \theta, \lambda) = \frac{GM_2}{r} \sum_{n=0}^{360} \left( \frac{a_2}{r} \right)^n \sum_{m=-n}^n \left( \frac{GM_1}{GM_2} \right) \left( \frac{a_1}{a_2} \right)^n \bar{C}_{nm} \bar{Y}_{nm}(\theta, \lambda)$$

where the scaled coefficients will be expressed as:

$$\bar{E}_{nm} = (GM_1/GM_2) * (a_1/a_2)^n C_{nm} = \text{scale}(n) C_{nm}$$

Thus:

$$V_1(r, \theta, \lambda) = \frac{GM_2}{r} \sum_{n=0}^{\infty} \left( \frac{a_2}{r} \right)^n \sum_{m=-n}^n \bar{E}_{nm} \bar{Y}_{nm}(\theta, \lambda)$$

Now, with a common  $GM_2$  and  $a_2$  value "out front", we can now write the formula of the disturbing potential as:

$$T(r, \theta, \lambda) = \frac{GM_2}{r} \sum_{n=0}^{\infty} \left( \frac{a_2}{r} \right)^n \sum_{m=-n}^n [\bar{E}_{nm} - \bar{D}_{nm}] \bar{Y}_{nm}(\theta, \lambda)$$

Of primary importance here is the fact that the degree zero term is non-zero if  $GM_1 \neq GM_2$ . In the case of  $GM_1$  for OSU91A (Rapp et al. 1991) versus  $GM_2$  of GRS80 (Moritz 1992), this effect is on the order of 1 meter, in geoid undulation.

Of secondary importance is the scaling of the coefficients. The scale factors are on the order of  $10^{-4}$ , and this effect has been shown in some of our tests to have an RMS of 0.3 mm, with min/max values of -0.3 mm and +0.5 mm for the geoid. While any one effect of sub-mm level will not adversely effect our results, we feel that the number of such approximations that currently exist in the theory need to be removed to prevent the possibility of their combined effects being noticeable at the 1 cm level. It should be noted that this effect of properly scaling

the coefficients is not encompassed in a simple geometric transformation, but represents a fundamental correction to the way that a spherical harmonic expansion is evaluated.

In general remarks, we are also careful about the difference between  $\partial/\partial r$  and  $\partial/\partial h$ . The difference between the two derivatives will have small (about 5 ppm), but calculable effects, on quantities of interest (gravity anomalies, upward derivatives of the height anomaly, etc...). And, wherever possible, exact (closed) formulas or iterations are performed (for example, computing the flattening from  $J_2$ ,  $\omega$ ,  $GM$ , and  $a$ ), rather than using any approximate formulas. Considering the speed with which iterations can be performed, we felt it was best to remove as many approximate formulas as was reasonably possible.

Next, we consider the issue that geopotential coefficients do not accurately represent the behavior of the actual geopotential interior to the Earth's surface. This problem was raised in Rapp (1992), and amplified in Rapp (1996). Basically, one must evaluate the geopotential on or above the Earth's surface, and then develop the geoid undulation from that computation. It is convenient, therefore, to first compute height anomalies,  $\zeta$ , and then convert them to geoid undulation,  $N$ , by means of Eq. (8-10) of Heiskanen and Moritz (1967)

$$N = \zeta + \frac{\Delta g_B}{\gamma} h$$

where:

$\Delta g_B$  simple (non-terrain corrected) Bouguer anomaly

A popular choice in geopotential coefficient evaluation is the Clenshaw summation approach described in Tscherning, et al (1983). This implementation, however, must reform certain sums whenever the geocentric radius,  $r$ , varies. To aid in computational efficiency, Rapp (1996) computes the height anomaly on the ellipsoid,  $\zeta_o$ , and then upward continues to the surface by the orthometric height,  $H$ ,

$$\zeta_p = \zeta_o + \partial\zeta/\partial r H$$

In an enhancement to this approach, we perform the upward continuation by

$$\zeta_p = \zeta_o + \partial\zeta/\partial h h$$

where, after suppressing a negligible  $\theta$  dependence (0.1 ppm),

$$\partial\zeta/\partial h = \partial(T/\gamma)/\partial h = [(1/\gamma) \partial T/\partial r \partial r/\partial h - (T/\gamma^2) \partial\gamma/\partial h]$$

and where ellipsoidal height,  $h$ , is established by  $H$  and a preliminary geoid height,  $N$ . Note that the second term, which contains the normal gravity gradient,  $\partial\gamma/\partial h$ , can be of the same magnitude as the first term.

As additional confirmation that some type of “upward/downward” procedure is needed to establish accurate geoid heights interior to the Earth’s surface, we compare the geoid heights computed from 2497 GPS benchmarks to the geoid heights computed from the X01 model. In Figure 1a, the X01 coefficients were directly evaluated at a geocentric radius,  $r_N$ , which is continually re-evaluated to conform to the geoid surface. In Figure 1b, our enhanced “upward/downward” procedure is followed. Both figures incorporate the  $GM$  and  $a$  variations discussed earlier. Comparison of the plots demonstrate clear height dependent error in Figure 1a when one attempts to directly compute the geoid undulations interior to the Earth’s surface.

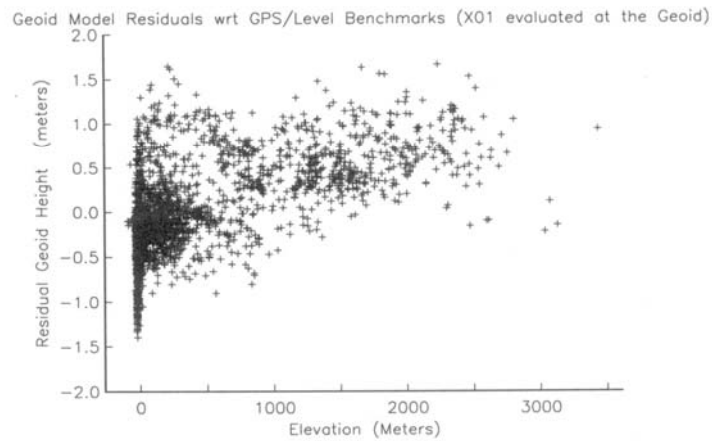


**Figure 1a: Geoid model residuals to GPS/benchmark geoid heights: X01 model evaluated at the geoid surface.**

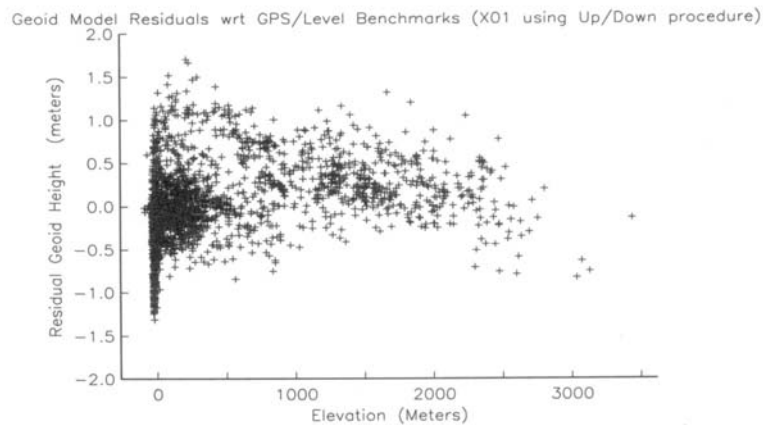


**Figure 1b: Geoid model residuals to GPS/benchmark geoid heights: X01 evaluated using the Upward/Downward procedure.**

## The GPS Benchmark Data Set

NGS is engaged in a project to establish a high accuracy Federal Base Network (FBN), and an associated Cooperative Base Network (CBN), through nationwide measurement of GPS baselines to 1 ppm accuracy or better. In the course of this survey effort, many of those FBN/CBN points are established on NAVD 88 optically leveled benchmarks. Figure 2 displays the locations of 2497 points that are leveled benchmarks with NAVD 88 Helmert orthometric heights, and which have GPS measured ellipsoidal heights in the NAD 83 (86) reference system as of March 1996. The irregular distribution illustrates the state-by-state approach to the surveying, and the different levels of state participation.

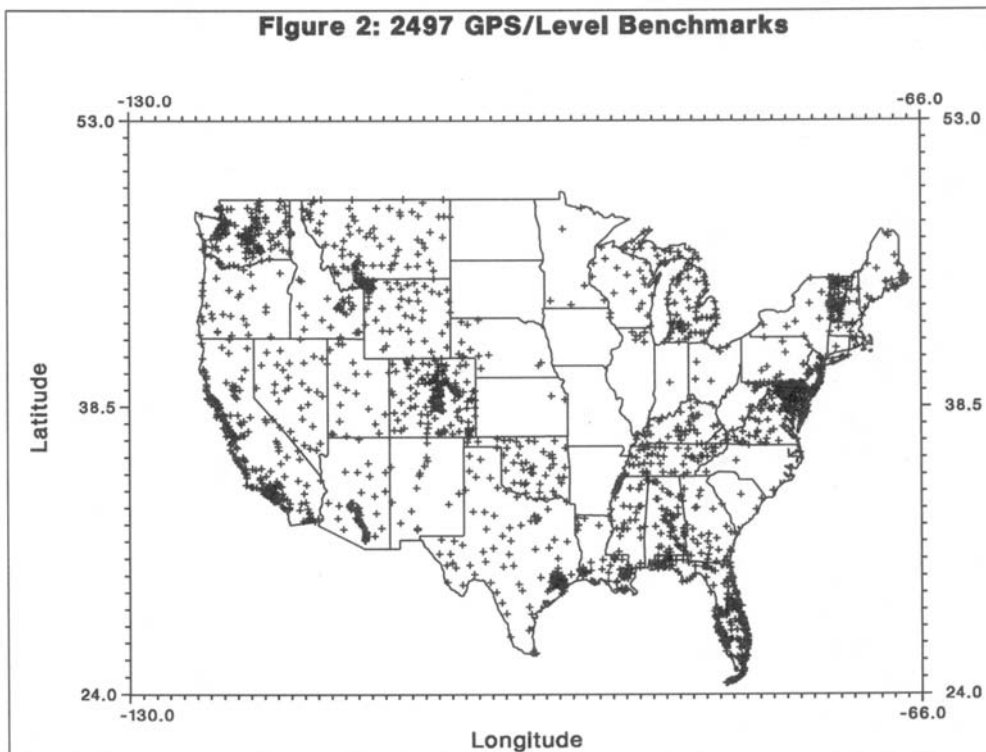


**Figure 2: 2497 Leveled Benchmarks with NAVD 88 Helmert Orthometric Heights and GPS Ellipsoidal Heights in the ITRF93(1995.0) Reference System.**

For the purposes of the preliminary model evaluation, the NAD 83 (86) coordinates are converted into the ITRF93(1995.0) reference frame. The transformation was performed using parameters established by Steve Frakes, National Geodetic Survey. These parameters are summarized in Table 1. In this paper, all ellipsoid heights are expressed relative to the GRS80 normal ellipsoid in the ITRF93(1995.0) frame.

$\Delta X$	-0.9769	$\pm 0.0166$	m
$\Delta Y$	+1.9392	$\pm 0.0137$	m
$\Delta Z$	+0.5461	$\pm 0.0141$	m
$\omega_x$	-0.0264	$\pm 0.0006$	arc sec
$\omega_y$	-0.0101	$\pm 0.0005$	arc sec
$\omega_z$	-0.0103	$\pm 0.0004$	arc sec
scale	-0.0068	$\pm 0.0017$	ppm

The NAVD 88 datum is expressed in Helmert orthometric heights, and was computed in 1991. The network contains over 1 million kilometers (km) of leveling at precisions ranging from 0.7 to 3.0 mm/ $\sqrt{\text{km}}$ , and incorporates corrections for rod scale, temperature, level collimation, astronomic, refraction, and magnetic effects (Zilkoski et al. 1992). The NAVD 88 datum was realized by a single datum point, Father Point/Rimouski, in Quebec, Canada. It must be mentioned that there is no guarantee that the NAVD 88 datum coincides with a given normal potential,  $U_0$ . For example, Rapp (1996) found a mean offset for the NAVD 88 datum of -34 cm relative to a  $U_0$  established by  $a=6378136.59$ . For additional details on the GPS benchmark data set, please refer to Milbert (1995).

### High Resolution Geoid Computation and Evaluation

The computation of the high resolution geoid models is based on the use of the Fast Fourier Transform (FFT) to evaluate Stokes equation. As described in Schwarz et al. (1990), a bandwidth-limited signal is needed for input to the FFT convolution. This mandates the use of a remove, compute, and restore procedure; where gravity anomalies from a global geopotential model are subtracted from gravity anomaly data, followed by convolution of the residual anomalies into residual geoid height, and then followed by restoration of geoid heights from that same geopotential model. Such an approach was used in the GEOID90 and GEOID93 computations for the United States (Milbert 1991, Milbert and Schultz 1993).

For the test model evaluation, a standard grid of terrain corrected, Bouguer anomalies was generated. Now, any gridding data set is subject to aliasing in the presence of high-frequency signal. To remove as much predictable, high-frequency content as possible, gridding is performed on terrain corrected, Bouguer anomalies,  $\Delta g_{\text{TB}}$ . For anomalies on land

$$\Delta g_{\text{TB}} = g + \frac{2\gamma_a}{a} [1 + f + m + (-3f + \frac{5}{2}m) \sin^2\phi] H - 3 \frac{\gamma_a}{a^2} H^2 - \gamma + A + C - 0.1119H$$

where

$$A = 0.8658 - 9.727 \cdot 10^{-5} H + 3.482 \cdot 10^{-9} H^2$$

and

$g$	surface gravity, tide corrected, IGSN71 system (mgals)
$H$	orthometric height, NAVD 88 datum (meters)
$\gamma$	normal gravity on ellipsoid, GRS80 (Somigliana's formula) (mgals)
$A$	atmospheric correction (Wichiencharoen 1982) (mgals)
$C$	terrain correction from 30" elevation grid (mgals)
$\phi$	geodetic latitude, NAD 83 (86) datum
$a$	semi-major axis, GRS80 (6378137 meters)
$\gamma_a$	normal gravity at equator, GRS80 (978032.67715 mgals)
$f$	ellipsoid flattening, GRS80 (0.00335281068118)
$m$	0.00344978600308 (GRS80)
$\rho$	density of topographic masses (2.67 gm/cm <sup>3</sup> )
$G$	gravitational constant
$R$	mean radius of the earth
$\psi$	spherical distance

The gridding algorithm uses a method of continuous curvature splines in tension (Smith and Wessel 1990) with tension parameter  $T_B = 0.75$ . The method is one which honors the data and does not display large oscillations in areas without data coverage. The standard Bouguer grid is a 3' by 3' regular grid extending from 24°N to 53°N and 230°E to 294°E (66°W to 130°W), and contains 581 rows and 1281 columns. All anomalies are prefiltered by computing mean value and mean location of the anomalies in 3' x 3' cells centered over the regular 3' latitude and longitude intersections. This prefiltering step is recommended by Smith and Wessel to reduce spatial aliasing effects prior to gridding.

Since we are using Stokes theory to compute the geoid, we require gravity anomalies on the geoid surface, rather than at the Earth's surface. We adopt Helmert's second method of condensation to regularize the problem and include the indirect effect with Grushinsky's formula

$$N = \frac{R}{4\pi\gamma} \iint_{\sigma} (\Delta g_{TB} + 0.1119H) S(\psi) d\sigma - \frac{\pi G \rho H^2}{\gamma}$$

where Stokes function is

$$S(\psi) = \frac{1}{\sin \frac{\psi}{2}} - 4 - 6 \sin \frac{\psi}{2} + 10 \sin^2 \frac{\psi}{2} - (3 - 6 \sin^2 \frac{\psi}{2}) \ln(\sin \frac{\psi}{2} + \sin^2 \frac{\psi}{2})$$

This setup is solved in a remove-compute-restore procedure using the FFT formulation of Strang van Hees (1990),

$$\Delta g_+ = (\Delta g_{TB} + 0.1119H) - \Delta g'_{360}$$

$$N_+ = \frac{R\Delta\phi\Delta\lambda}{4\pi\gamma} F^{-1}[F(\Delta g_+ \cos\phi_Q) F(S(\phi_P - \phi_Q, \lambda_P - \lambda_Q))]$$

$$N = N_+ + N'_{360}$$

where

$\Delta g_+$	high-frequency part of gravity anomalies
$\Delta g'_{360}$	geopotential model gravity anomalies at geoid surface
$\Delta\phi, \Delta\lambda$	grid spacing
$F, F^{-1}$	direct and inverse, two-dimensional, Fourier transforms
$N_+$	high-frequency part of geoid undulations
$N'_{360}$	geopotential model geoid undulations at geoid surface

and, where Stokes function,  $S$ , is evaluated with a mean latitude,  $\phi_m$ , and the approximation,

$$\sin^{1/2}\psi \doteq [\sin^2 \frac{1}{2}(\phi_P - \phi_Q) + \sin^2 \frac{1}{2}(\lambda_P - \lambda_Q) (\cos^2 \phi_m - \sin^2 \frac{1}{2}(\phi_P - \phi_Q))]^{1/2}$$

The input grid,  $\Delta g_+$ , (580 rows, 1280 columns) had 50% zero padding on all four edges to eliminate the effect of cyclic convolution (Gleason 1990). No tapering of  $\Delta g_+$  was performed, since the long wavelength part has already been removed. The FFT subroutine has an option which exploits the Hermitian symmetry resulting from real valued grids. Thus, doubled computation speed and storage efficiency was obtained without resorting to Hartley transforms.

An important issue must be mentioned at this point. The geopotential model geoid undulations,  $N'_{360}$ , are evaluated at the geoid surface. From the results of Figures 1a and 1b, it is seen that these geoid heights are biased. However, the Stokes procedure described above will remove that height dependent error if the gravity anomalies,  $\Delta g'_{360}$ , are also evaluated in a fashion consistent with the geoid undulations. Since it is not convenient to apply some form of “upward/downward” procedure to the gravity anomalies, we choose to evaluate both geoid and anomalies at the geoid surface. The key point is that we are consistent in our choice of surface for coefficient evaluation.

As a formal demonstration, consider Stokes equation written in a remove, compute, and restore procedure:

$$N = \frac{R}{4\pi\gamma} \iint_{\sigma} \Delta g S(\psi) d\sigma = \frac{R}{4\pi\gamma} \iint_{\sigma} (\Delta g - \Delta g'_{360}) S(\psi) d\sigma + \frac{R}{4\pi\gamma} \iint_{\sigma} \Delta g'_{360} S(\psi) d\sigma$$

The term on the right formulates the  $\delta N$ , which must be restored, as a function of the model gravity anomalies,  $\Delta g'_{360}$ , that were removed. Expanding Stokes function in Legendre polynomials and the gravity anomalies in terms of the harmonic coefficients yields

$$\delta N = \frac{R}{4\pi\gamma} \iint_{\sigma} \left[ \frac{GM}{r} \sum_{n=2}^{360} \left( \frac{a}{r} \right)^n \left( \frac{n-1}{r} \right) \sum_{m=-n}^n \bar{F}_{nm} \bar{Y}_{nm}(\theta, \lambda) \right] \left[ \sum_{n=2}^{\infty} \frac{2n+1}{n-1} P_n(\cos \psi) \right] d\sigma$$

where  $\bar{F}_{nm} = \bar{E}_{nm} - \bar{D}_{nm}$ . Perform the multiplication, exchange the order of the sums and integrals, under a standard assumption of convergence, combine terms, and invoke the orthogonality relationships of Legendre polynomials. After algebra, the equation above will simplify into

$$\delta N = \frac{GM}{r\gamma} \sum_{n=2}^{360} \left( \frac{a}{r} \right)^n \sum_{m=-n}^n \bar{F}_{nm} \bar{Y}_{nm}(\theta, \lambda)$$

if the leading  $R$  before the integral is taken to be  $r$ . The equation above is equivalent to  $N'_{360}$ . Other than the  $R=r$  requirement of the lead term, the development did not invoke any specific surface mandated by a remove, compute, and restore procedure. The development did show the consistent  $N'_{360}$  and  $\Delta g'_{360}$  expressions.

The high resolution geoid models are derived from four data sources: point gravity measurements, satellite altimetry-derived gravity anomalies, digital terrain, and geopotential coefficients. A few remarks are appropriate. About 1.8 million gravity points, both ship and terrestrial, went into the gridding. These data were a combination of NGS-held data and quality controlled data from the Defense Mapping Agency. The satellite altimetry-derived gravity anomalies were computed by Sandwell and Smith (1996). These were included in gravity void regions where depths exceeded 500 meters and which were 200 km or more from land. The digital terrain data came primarily from the 30" point topography database, TOPO30, distributed by the National Geophysical Data Center (Row and Kozleski 1991). The 30" elevation set was used to compute both terrain corrections, and 3' x 3' mean elevations. And, of course, the preliminary geopotential models, X01 through X05, were used as the coefficient sources. We denote the resultant high resolution models as 9620 through 9624, respectively.

We explore the general properties of the solutions by computing geoid height residuals,  $e$ , in the sense of

$$e = \text{high-res. geoid height} - (\text{ITRF93(1995.0) ellipsoid height} - \text{NAVD 88 orthometric height}).$$

Tilted plane models are fit to the 2497 residuals and are summarized in Table 2.

Model	Offset (cm.)	Tilt (ppm)	RMS about plane (cm)	Azimuth (deg)
9620	-4.58	0.04	35.07	293
9621	-5.90	0.06	36.14	317
9622	-2.07	0.05	36.14	319
9623	-2.05	0.06	36.56	321
9624	-2.05	0.05	36.52	321

**Table 2. Tilted plane fits to 2497 high resolution geoid model residuals .**

These results begin to indicate model differences. The average offsets suggest that X01 and X02 used differing data and/or procedures from X03, X04, and X05. The small magnitude of the offsets must be considered in the context of the comparisons. The GRS80 normal ellipsoid is used to express the ellipsoidal heights, the normal gravity, and the high resolution geoid models. Thus, the small offsets are not inconsistent with the -34 cm found by Rapp (1996).

Next, following the approach of Milbert (1995), smoothed residual surfaces are computed by means of collocation for all 5 high resolution models. Empirical covariance functions were fit to the covariance statistics of the detrended geoid residuals. The fits were made using a simple function of the form

$$C=C_0e^{(-d^2/L^2)}$$

where

- $d$  = the spherical distance between points (km)
- $L$  = characteristic length (km)
- $C_0$  = function variance ( $m^2$ )

The function fits were virtually identical, with only minor variations of  $L = 485$  km and  $C_0 = (0.31)^2 m^2$ . As was seen in Milbert (1995), the residual error is sizable and correlated over a long length scale. The detrended residual error,  $\hat{s}$ , is predicted on a 30' x 30' grid using least-squares collocation with noise (Moritz 1980, p.102-106). The prediction formula is

$$\hat{s} = C_{st}(C_{tt} + C_{nn})^{-1}$$

where

- $C_{tt}$  = signal covariance between observations
- $C_{st}$  = signal covariance between predicted signal and observations
- $C_{nn}$  = covariance of random measuring errors, taken as diagonal and constant:  $C_{nn}=s_o^2 I$

Before the grids are computed, the prediction process is iterated to establish a value of  $s_o^2$  consistent with the residual misfit about the predictions. It was found the RMS of residuals from the prediction step matched the assigned noise when  $s_o^2 = (5.6)^2 cm^2$  for the  $n=2497$  points. The trends reported in Table 2 were restored to the detrended signal grids, resulting in the final corrector surface grids (adjusted in sign to provide an additive correction).

Figure 3 portrays a trend surface that, when added to the 9622 geoid model, will directly relate ITRF93(1995.0) ellipsoid heights and NAVD 88 Helmert orthometric heights. In viewing this figure it must be recalled that the GPS benchmarks used to develop this grid all lie within the U.S. borders; and that highs or lows in the oceans or in other countries are extrapolations, and are not reliable. In the interests of concision, the trend surfaces for the other 4 models are not displayed, since they appear almost identical.

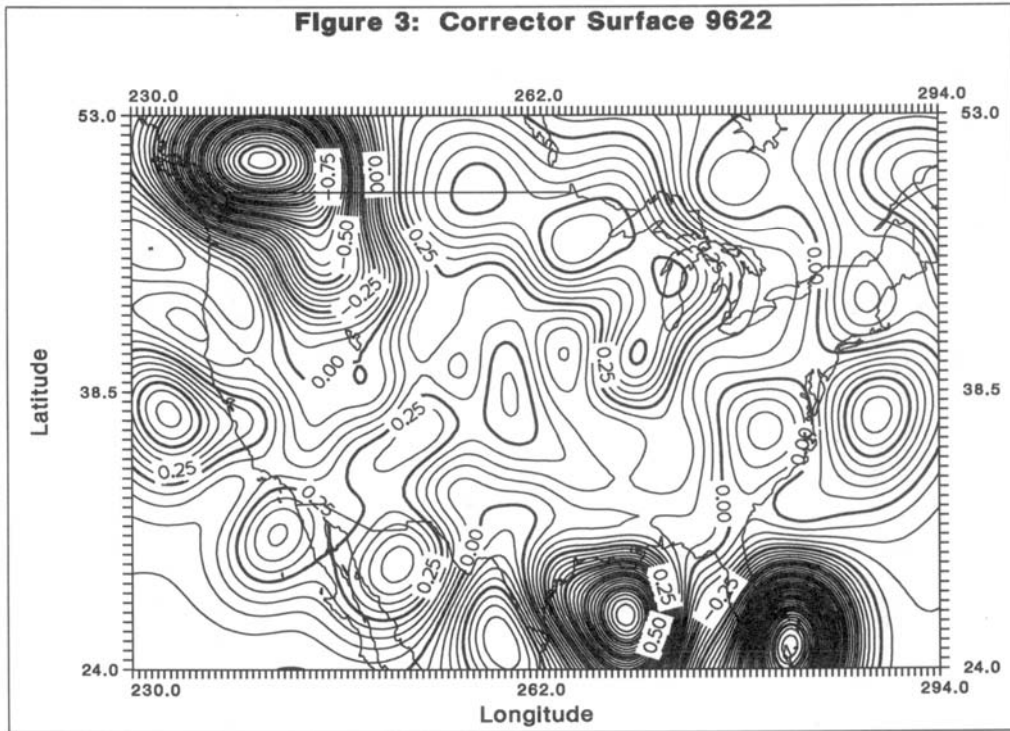


**Figure 3: Trend Surface to Relate High-Resolution Model 9622 to GPS Benchmarks (Contour Interval = 0.05 m).**

As part of the evaluation process, we computed all possible combinations of the residual trend surface differences, 10 in all. These are reproduced in Figures 4a through 4j. Inspection of the combinations indicate that the 9623 and 9624 models were virtually identical, and that 9622 was very close to the 9623 model. (One must discount features in the GPS benchmark void areas.) It is also seen that model 9621 shows some departures from 9622, and that 9620 is the most different of all the models. These results confirm the similarities of the 9622, 9623, and 9624 models, and also suggest that both 9620 and 9621 are distinct from them and are distinct from one another.

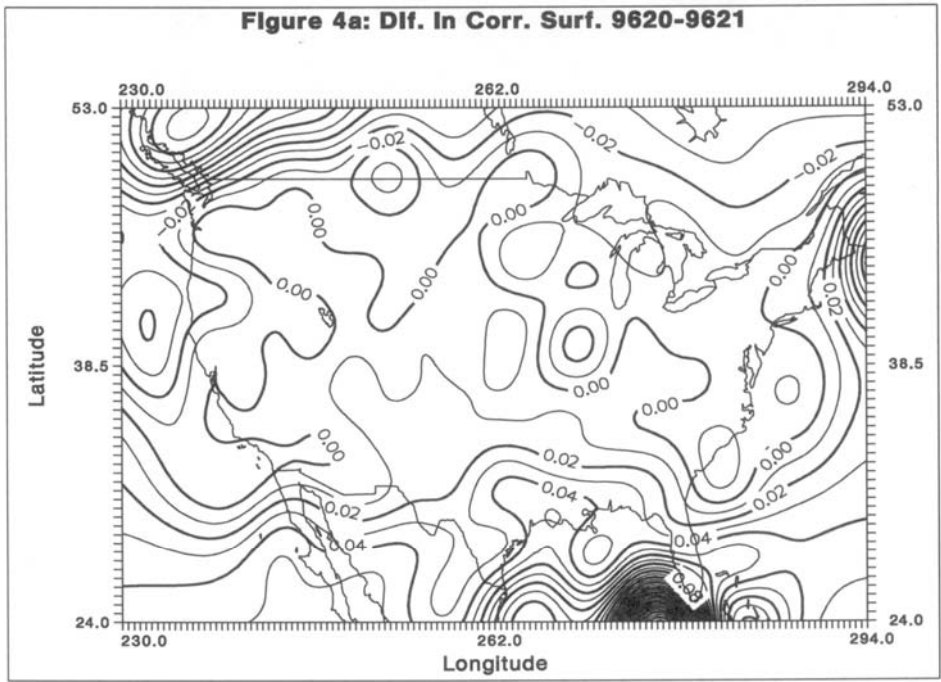


Figure 4a: Differences between Trend Surfaces 9620 and 9621 (Contour Interval = 0.01 m)

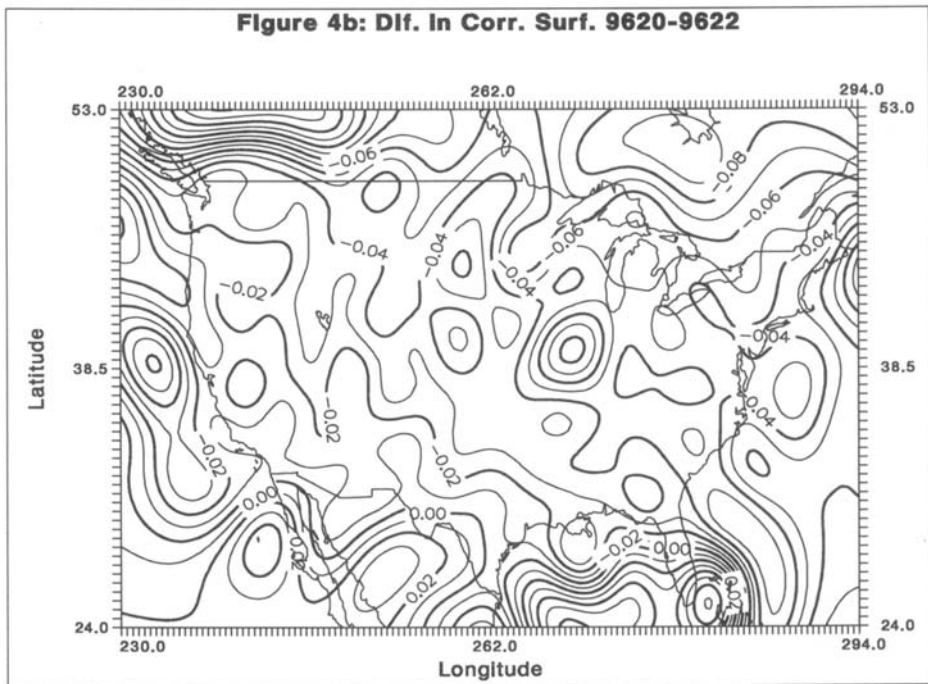


Figure 4b: Differences between Trend Surfaces 9620 and 9622 (Contour Interval = 0.01 m)

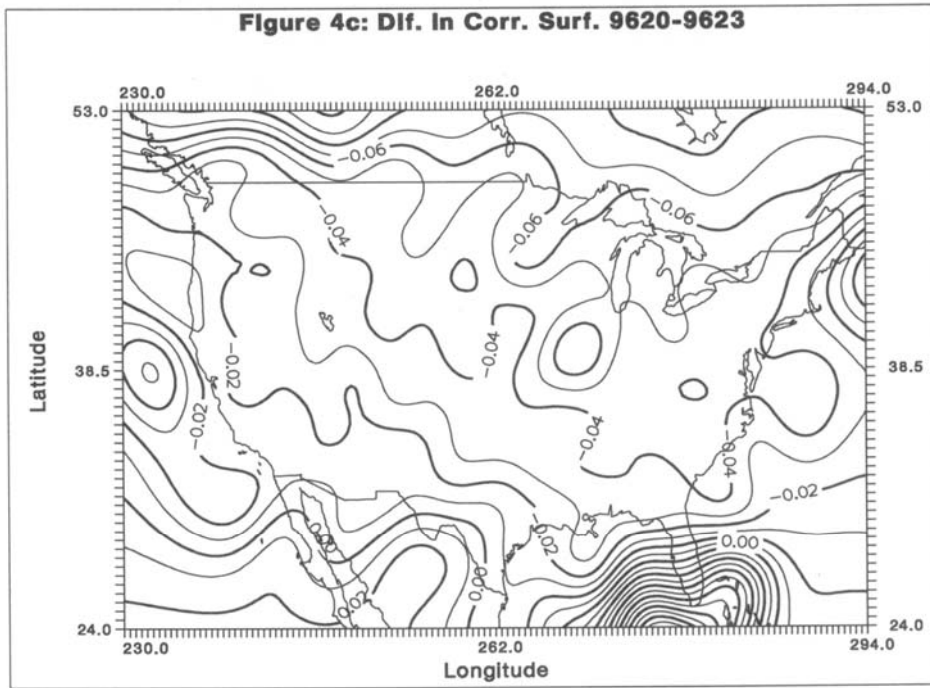


Figure 4c: Differences between Trend Surfaces 9620 and 9623 (Contour Interval = 0.01 m)

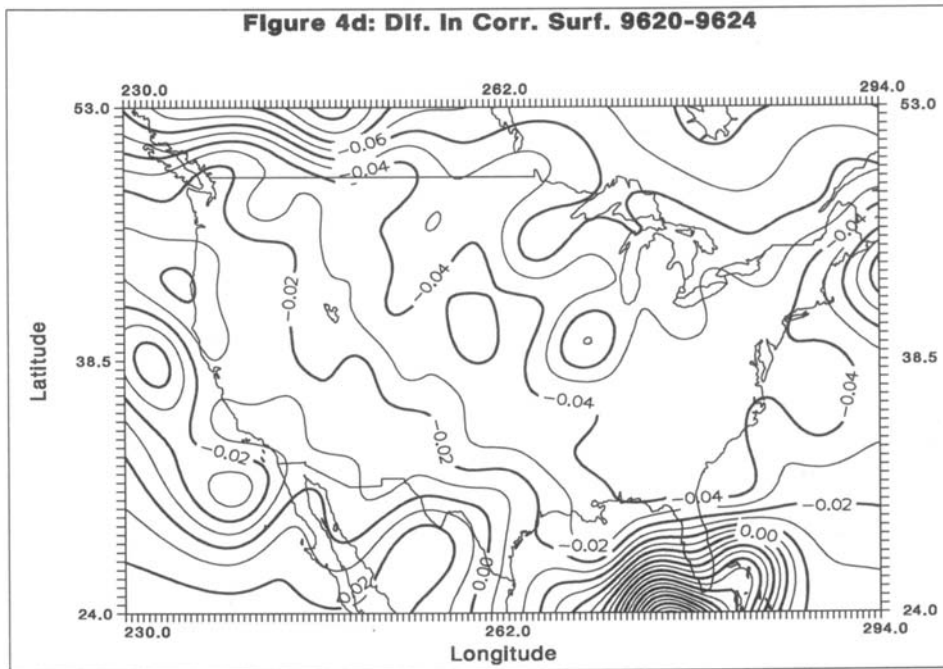


Figure 4d: Differences between Trend Surfaces 9620 and 9624 (Contour Interval = 0.01 m)

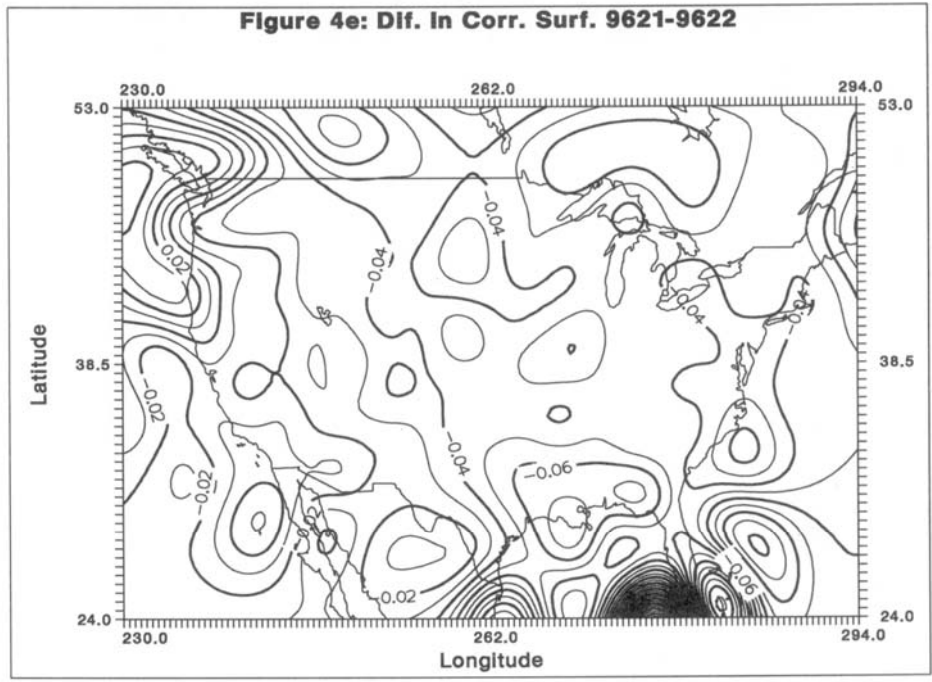


Figure 4e: Differences between Trend Surfaces 9621 and 9622 (Contour Interval = 0.01 m)

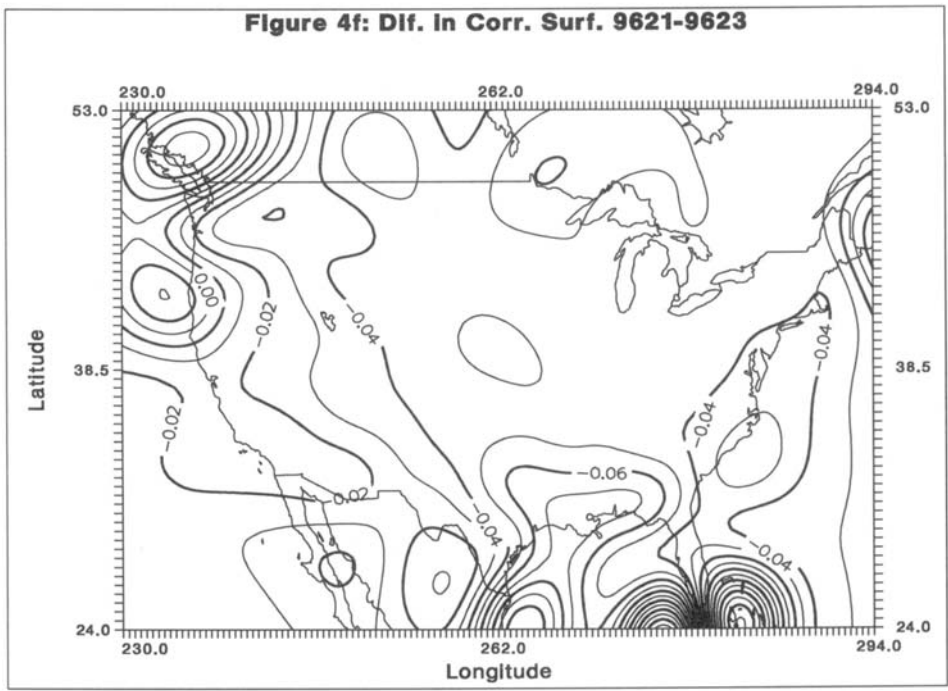


Figure 4f: Differences between Trend Surfaces 9621 and 9623 (Contour Interval = 0.01 m)

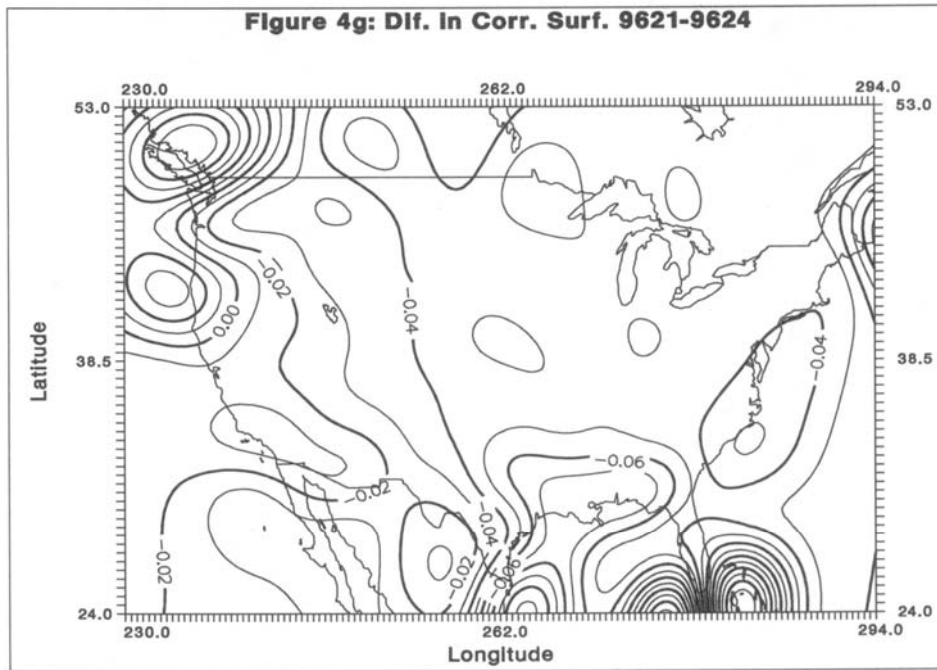


Figure 4g: Differences between Trend Surfaces 9621 and 9624 (Contour Interval = 0.01 m)

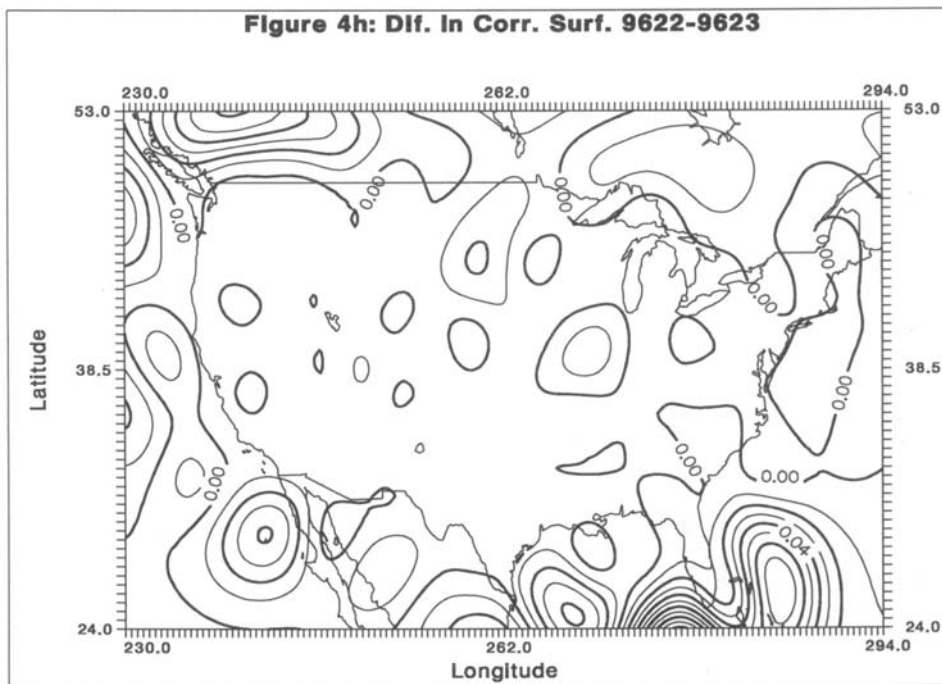


Figure 4h: Differences between Trend Surfaces 9622 and 9623 (Contour Interval = 0.01 m)

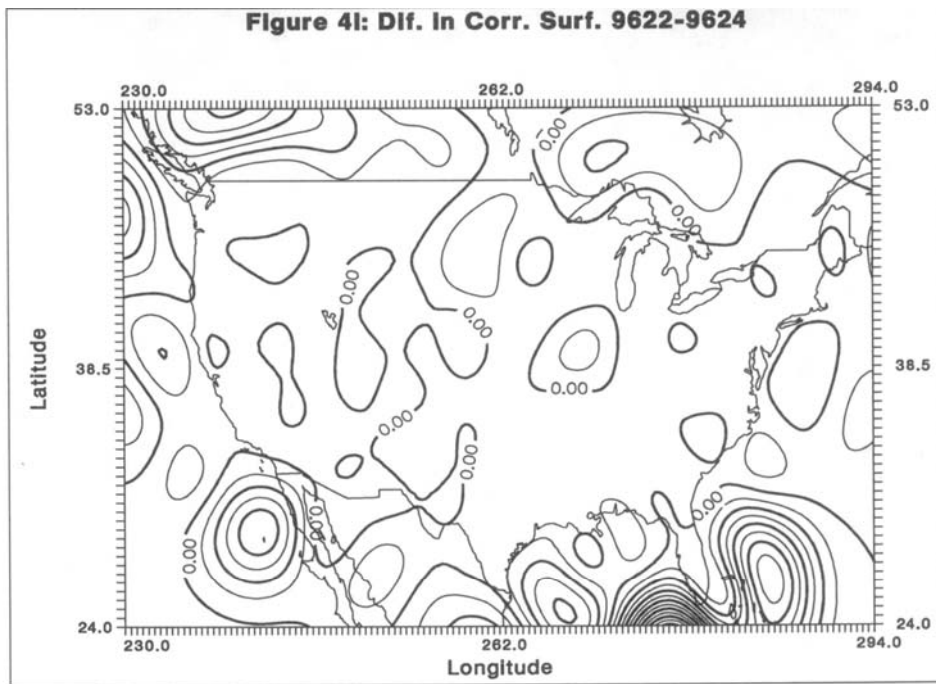


Figure 4i: Differences between Trend Surfaces 9622 and 9624 (Contour Interval = 0.01 m)

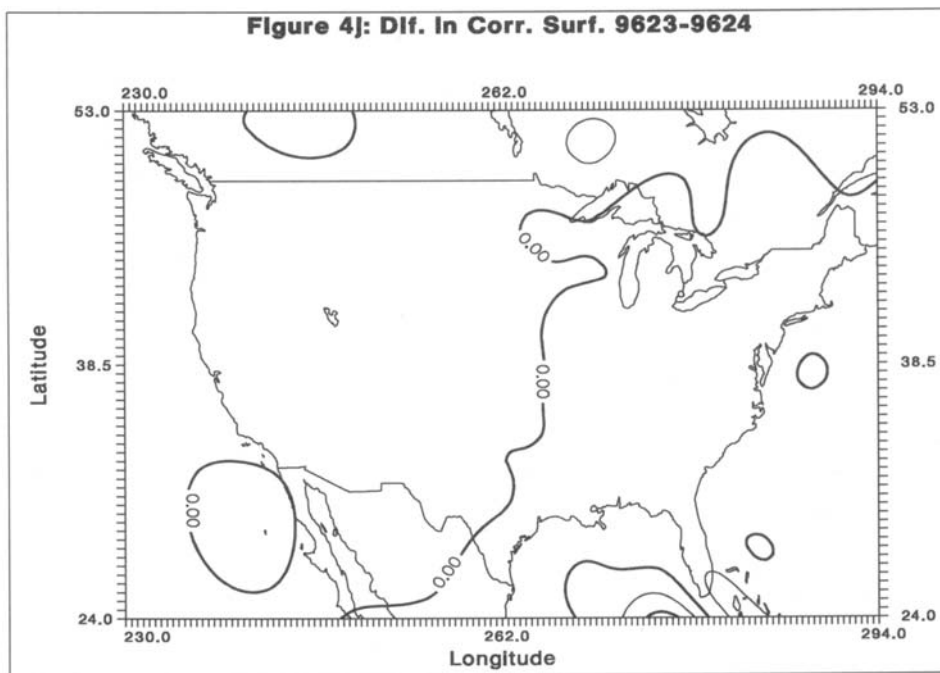
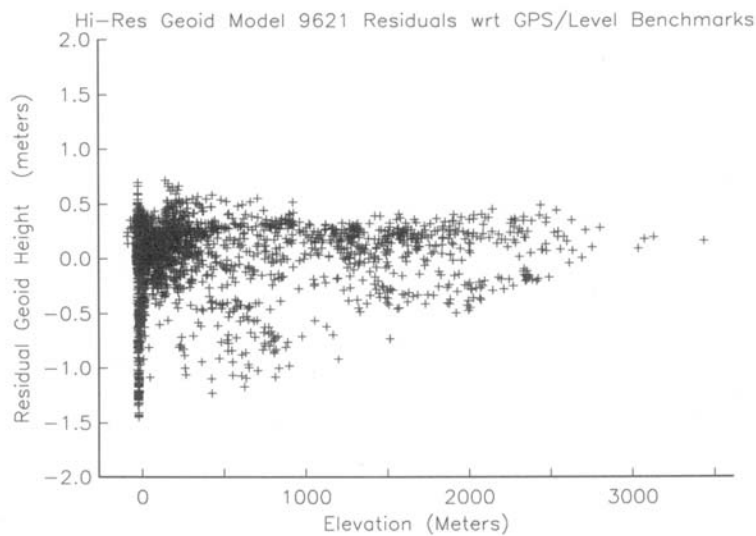


Figure 4j: Differences between Trend Surfaces 9623 and 9624 (Contour Interval = 0.01 m)

At this point it is helpful to review particular features seen in the trend surfaces. A tilt is evident in Florida, and it is virtually the same in all models. This effect has been observed with both the GEOID90 and GEOID93 models, as well as with numerous test models. Given the great care taken by the geopotential model computation team in the intercomparisons of marine gravity and altimetry derived gravity, and given the very flat topography of Florida, it is unlikely that the geoid models are the source of this feature. Further, since the GPS network is anchored to the Richmond VLBI site at the tip of Florida, it is also unlikely that the ellipsoid heights are biased in that region. The leveling is suspect. On the other hand, the tilt along the Gulf Coast is probably gravimetric in origin; and will be discussed later in this section.

A North-South tilt is also evident in Washington State. The source of this feature seems to be the terrain corrections computed from digital terrain data in southern British Columbia. We are working with the Geodetic Survey of Canada to resolve this problem. It is thought, however, that the mean gravity anomalies used to compute the preliminary geopotential models are accurate. The tilt is seen to blend into an elongated feature over the northern Rockies. This raises some concern over possible height-dependent error.

As a different view of the models, we made scatter plots of the geoid height residuals relative to elevation. A sample for the 9621 model is given in Figure 5, since the scatter plots look similar. The dispersion of values near the zero elevation reflect the issues in Florida and the Gulf Coast noted earlier. No obvious height dependence is evident in Figure 5, unlike the effect seen in Figure 1a. However, overlays of the the 5 different scatter plots do show small variations that could have an elevation dependence.



**Figure 5: High Resolution Model 9621 Height Residuals to GPS Benchmark Geoid Heights**

In pursuit of this possibility, an exploratory GPS benchmark data set was formed by withholding the points in Florida south of 30°N, and by withholding the points north of 48°N in Washington State. The average offset, and the RMS about the offset are then computed. In addition, the offset and RMS are computed where data are withheld below 1000 m, below 1500 meters, and below 2000 meters in elevation. The statistics are grouped by model, ordered by ascending elevation, and displayed in Table 3. In addition, the differences in average offset, and second differences are displayed.

9620 Model (X01)	Cutoff (m)	n	RMS (cm)	Offset (cm.)	Diff	2nd-Diff
	0	2190	24.85	9.15		
	1000	448	23.99	6.58		
	1500	268	24.98	6.32	-0.26	
	2000	107	24.79	6.70	0.38	0.64
9621 Model (X02)	Cutoff (m)	n	RMS (cm)	Offset (cm.)	Diff	2nd-Diff
	0	2190	24.59	9.82		
	1000	448	23.76	7.50		
	1500	268	24.71	7.15	-0.35	
	2000	107	24.51	7.57	0.42	0.77
9622 Model (X03)	Cutoff (m)	n	RMS (cm)	Offset (cm.)	Diff	2nd-Diff
	0	2190	24.64	9.71		
	1000	448	23.77	7.07		
	1500	268	24.78	6.92	-0.15	
	2000	107	24.50	7.46	0.54	0.69
9623 Model (X04)	Cutoff (m)	n	RMS (cm)	Offset (cm.)	Diff	2nd-Diff
	0	2190	24.66	9.92		
	1000	448	23.78	7.38		
	1500	268	24.77	7.26	-0.12	
	2000	107	24.47	7.83	0.57	0.69
9624 Model (X05)	Cutoff (m)	n	RMS (cm)	Offset (cm.)	Diff	2nd-Diff
	0	2190	24.73	9.84		
	1000	448	23.83	6.97		
	1500	268	24.80	6.88	-0.09	
	2000	107	24.50	7.43	0.55	0.64

**Table 3. Geoid residual statistics ordered by elevation cutoff tolerance.**

Table 3 enables us to discern more about the computation of the preliminary models. The differences in the average offset between the 0 m elevation cutoff and the 1000 m cutoff are probably indicative of remaining systematic errors in the GPS benchmark or in the detail gravity data, rather than reflecting characteristics of the global models. We know that the average offset will contain NAVD 88 vertical datum error. We don't know what that error is, but we can expect that error to be constant with respect to elevation. Thus, we can expect a zero value for the *differences* in average offset. Height dependent effects will cause variations in the average offsets as the elevation cutoff is varied.

Looking at the offset difference column, we see that X03, X04, and X05 are distinct from X01 and X02. In fact, the close similarities suggest that X03, X04, and X05 are members of a family, perhaps controlled by some tuning parameter(s), such as anomaly weighting. And, it

seems that the models X03, X04, and X05 are provided in sequence; corresponding to monotonic changes in the hypothetical parameter.

At this stage it is seen that model 9624, computed from X05, displays the most uniform average offsets.

To close this section, a result was obtained that sets the stage for the next section of the report; where the models are directly compared against GPS benchmarks. Recall that in this section, the geopotential models are evaluated through high-resolution geoid models computed in a remove, compute, and restore procedure. One of the products of this procedure is the output grid from the FFT convolution, which we denoted,  $N_+$ . This grid contains the high-frequency part of the geoid (truncation or omission error), but also contains information about lower-frequency commission error.

One must interpret an  $N_+$  grid with caution. First, the grid, when added to the preliminary model geoid,  $N_{360}$ , will yield the co-geoid. One can think of the  $N_+$  grid as being biased by the indirect effect, since Faye anomalies were used in its computation. Second, our model geoids,  $N_{360}$ , were biased, since they were evaluated interior to the Earth. Therefore, our  $N_+$  grids will also contain that height-dependent bias. Despite these drawbacks, the  $N_+$  grid certainly contains useful information at lower elevations.

Figure 6 portrays a color shaded relief image of the  $N_+$  grid associated with the X02 model. Sixteen hues were allocated from the low of -1.5 m (magenta) to the high of +1.5 m (red). Sixteen levels of gray shading were added to give the effect of illumination from the East. The magnitudes of the grid actually ranged from -4.1 m to 2.8 m. Thus, values which exceed the  $\pm 1.5$  meter interval will “saturate” into the magenta or the red coloring. The grids from the other preliminary models look very similar.

Most noticeable is the large blue and magenta structure in the Rockies. Because of the bias issues discussed above, one can, at most, say that it hints at significant commission error in the Rockies. This issue will be explored in the next section.

Other features are interesting. The lows in Lake Superior may be due to our treatment of the elevations of the ship gravity data. The low in the Bermudas may also be related to our gravity data set, and will be investigated at a later stage. While the Bermudas feature does induce a tilt across Florida, it is localized to the south, and does not explain the complete amount of tilt we have seen in the past. In addition, some portion of the low seen in Washington State and southern British Columbia is due to currently unresolved problems with terrain corrections, discussed earlier.

On the other hand, the 0.5 m feature in the Central U.S., and the 1 m features in the Gulf of Mexico and off the Atlantic seaboard are less easily explained. These are regions of low elevations, and are rather broad. The data in the Gulf and near-shore Atlantic are ship gravity data. The altimeter-derived gravity anomalies from Sandwell and Smith (1996) were only used in the southern part of the Gulf and in the deep Atlantic. We suspect these particular features

may be due to preliminary model commission error; perhaps correlated with some sea surface (dynamic) topography effect in the ocean.

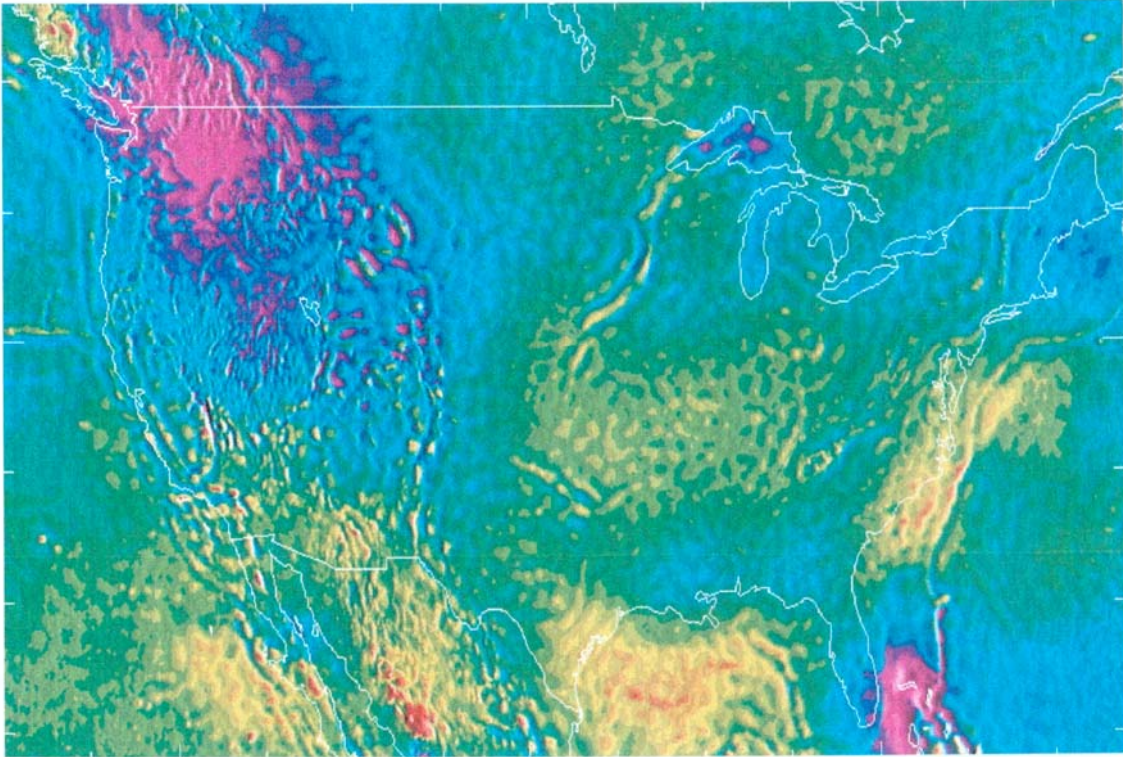


**Figure 6: High Frequency Component of Geoid Height for High-Resolution Model 9621 Relative to Preliminary Geopotential Coefficient Model X02.**

#### **Low Resolution Geoid Computation and Evaluation**

In this section, we compare geoid heights computed directly from the preliminary geopotential models against the GPS benchmark data set. While these statistics are very noisy, due to omission error, they can portray long wavelength commission error.

Five geoid grids at 3' x 3' spacing were computed from the X01 through X05 coefficients. All grids were computed with the “up/down” procedure, where the coefficients are evaluated at the ellipsoid, upward continued to the surface to form a height anomaly, and then converted “down” to a geoid height by means of Eq. (8-10) of Heiskanen and Moritz (1967). This last step is implemented as a 3' x 3' grid which has been low pass filtered to correspond to an  $n=360$

resolution. We emphasize that these geoid grids are *not* subject to the height-dependent error illustrated in Figure 1a.

Tilted plane models are fit to 2497 residuals about the low resolution geoid grids, and are summarized in Table 4.

<b>Model</b>	<b>Offset (cm.)</b>	<b>Tilt (ppm)</b>	<b>RMS about plane (cm)</b>	<b>Azimuth (deg)</b>
X01	-2.16	0.40	26.52	338
X02	1.02	0.32	29.77	336
X03	0.07	0.35	26.22	334
X04	0.43	0.35	25.99	335
X05	0.76	0.35	26.10	335

**Table 4. Tilted plane fits to 2497 low resolution geoid model residuals .**

These results are remarkable, in that they show a significant tilt to the Northwest. This confirms the suspicion that the large blue and magenta feature seen in the Rockies in Figure 6 is at least partly due to preliminary geopotential model commission error. It should be recalled that this tilt was not evident when the GPS benchmark residuals to the high-resolution geoid models were computed in Table 2. It appears that the high-resolution models remove not only omission error, but also commission error.

To produce an image for evaluation, smoothed residual surfaces were computed by means of collocation for all 5 low resolution models. Empirical covariance functions were fit to the covariance statistics of the detrended geoid residuals. The function fits were virtually identical, with only minor variations of  $L = 200$  km and  $C_0 = (0.21)^2$  m<sup>2</sup>. The trends reported in Table 4 were restored to the detrended predicted signal grids, resulting in the final smoothed residual surfaces. The surfaces for the 5 models were virtually identical, so only the result for model X01 is displayed in Figure 7.

The complex structure seen in Figure 7 is a representation of the preliminary model omission error as sampled by the GPS benchmarks. These small features can be reduced with more stringent smoothing, and should be ignored. Similarly, features in the oceans (e.g. near Florida) or beyond the U.S. borders should also be ignored, since those represent extrapolations. Further, the presence or absence of structure in the central U.S. has no meaning, due to the absence of GPS benchmarks.

However, an offset in the northern Rockies, relative to the plains, is evident in Figure 7. Unfortunately, shortages of GPS benchmarks in the central U.S., in the Carolinas, and south of Houston, Texas, make it difficult to comment on other features discussed in Figure 6. It is noteworthy that the tilt in Florida is still evident; a result consistent with a hypothesized problem in the level network.

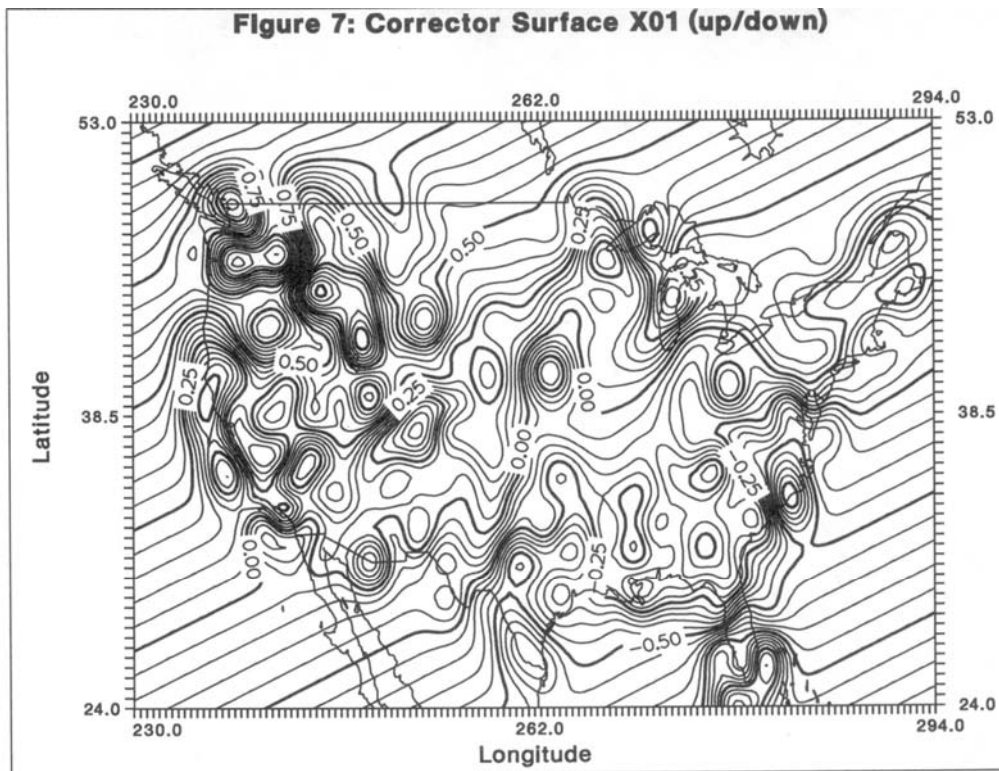


**Figure 7: Trend Surface to Relate Low-Resolution Geoid Model X01 to GPS Benchmarks (Contour Interval = 0.05 m).**

To further study the behavior of the preliminary models and the possibility of commission error in the Rockies, 505 GPS benchmarks in the region of 38°- 49°N and 230°- 255°E were extracted from the full data set. These points were then grouped into 500 m elevation cohorts, and statistics were computed. The statistics are grouped by model, ordered by ascending elevation, and displayed in Table 5. In addition, the differences in average offset, and, second and third differences are displayed. Only 15 GPS benchmarks are present in the “over 2500 m” cohort, and those statistics are not felt to be reliable.

X01 Model	Cohort	n	RMS (cm)	Offset (cm.)	Diff	2nd-Diff	3rd-Diff
	0- 500	138	46.67	70.05			
	500-1000	97	27.69	69.22			
	1000-1500	93	28.78	49.63	-19.59		
	1500-2000	91	31.17	35.16	-14.47	5.12	
	2000-2500	71	34.38	18.02	-17.14	-2.67	-7.79
	Over 2500	15	34.92	-23.29			
	-----						
	All	505	42.38	49.75			

<b>X02 Model</b>	<b>Cohort</b>	<b>n</b>	<b>RMS (cm)</b>	<b>Offset (cm.)</b>	<b>Diff</b>	<b>2nd-Diff</b>	<b>3rd-Diff</b>
	0- 500	138	37.41	66.00			
	500-1000	97	26.80	62.36			
	1000-1500	93	29.39	49.42	-12.95		
	1500-2000	91	35.50	38.88	-10.54	2.41	
	2000-2500	71	30.62	23.28	-15.60	-5.06	-7.47
	Over 2500	15	37.65	-4.00			
	All	505	37.26	49.28			
<b>X03 Model</b>	<b>Cohort</b>	<b>n</b>	<b>RMS (cm)</b>	<b>Offset (cm.)</b>	<b>Diff</b>	<b>2nd-Diff</b>	<b>3rd-Diff</b>
	0- 500	138	49.90	73.29			
	500-1000	97	30.50	69.54			
	1000-1500	93	27.14	45.97	23.57		
	1500-2000	91	32.09	36.37	9.59	13.98	
	2000-2500	71	32.07	19.11	-17.26	-7.67	-21.65
	Over 2500	15	36.65	-16.48			
	All	505	43.45	50.60			
<b>X04 Model</b>	<b>Cohort</b>	<b>n</b>	<b>RMS (cm)</b>	<b>Offset (cm.)</b>	<b>Diff</b>	<b>2nd-Diff</b>	<b>3rd-Diff</b>
	0- 500	138	48.76	72.19			
	500-1000	97	31.32	69.65			
	1000-1500	93	28.26	44.36	-25.29		
	1500-2000	91	32.13	35.78	-8.58	16.70	
	2000-2500	71	31.75	20.01	-15.77	-7.19	-23.89
	Over 2500	15	36.04	-12.59			
	All	505	42.96	50.16			
<b>X05 Model</b>	<b>Cohort</b>	<b>n</b>	<b>RMS (cm)</b>	<b>Offset (cm.)</b>	<b>Diff</b>	<b>2nd-Diff</b>	<b>3rd-Diff</b>
	0- 500	138	49.27	71.02			
	500-1000	97	31.76	69.20			
	1000-1500	93	28.49	42.93	-26.27		
	1500-2000	91	32.98	34.90	-8.03	18.24	
	2000-2500	71	29.93	18.54	-16.36	-8.33	-26.57
	Over 2500	15	35.05	-12.43			
	All	505	43.14	49.13			

**Table 5. Geoid residual statistics ordered by 500 m elevation cohorts.**

Table 5 supports many of the conclusions developed from analysis of Table 3. Models X03 through X05 seem to be members of a family, and seem ordered relative to some tunable parameter(s). Models X01 and X02 are distinct from that family, and from one another. Unlike the situation in Table 3, some interpretation can be applied to the average offset column. While we do not know the true value of the datum offset associated with NAVD 88 (in GRS80), the high-resolution geoid model results in Table 3 indicate that it is a value closer to 10 cm than to 40 cm. This leads us to prefer models with a smaller average offset, since we feel the offset is partly due to commission error. Models X02 and X05 look best. In general, model X05 has smaller offsets per cohort, but shows greater height dependence of those offsets when compared to X02. The smaller RMS about the average offsets of model X02 is also attractive.

## Conclusions and Recommendations

Differencing the geoid grids computed from the preliminary geopotential model coefficients show the test models to be very similar. So it is clear that any of the test models represents a major advance over currently available geopotentials. With this said, we have a preference for models X05 and X02, with a very slight edge towards X05. This preference is based on criteria of low height dependence of geoid residuals, low average offsets of the residuals (for the case of the low-resolution models), and low RMS values. It is interesting that these criteria lead to the same model preferences irrespective of the high-resolution or the low-resolution approach.

Since it is likely that the final model will not be any one of the beta test models, it is worthwhile to state that an ideal model would combine characteristics from X02 and X05. However, all the preliminary models share the commission error seen in the region  $38^{\circ}$ - $49^{\circ}$ N,  $230^{\circ}$ - $255^{\circ}$ E. If this effect could be lessened, then the final model would be even better.

## Acknowledgments

Work of this scope required the contributions of dozens of individuals. Virtually every employee of the National Geodetic Survey has assisted in this effort. The gravity data set, the NAVD 88 project, and the GPS state upgrade program were vital to this study. The Defense Mapping Agency (DMA) provided a major portion of the NGS land gravity data set, and was instrumental in creation of the various 3" and 30" elevation grids in existence. Dr. Walter Smith, NOAA, provided the altimeter-derived gravity anomalies.

## References

Gleason, D.M., 1990: Obtaining Earth surface and spatial deflections of the vertical from free-air gravity anomaly and elevation data without density assumptions. *J. Geophys. Res.*, 95(B5), 6779-6786.

Heiskanen, W.A. and H. Moritz, 1967: *Physical Geodesy*. W.H. Freeman, San Francisco, 364 pp.A46-55.

Milbert, D.G., 1995: Improvement of a high resolution geoid height model in the United States by GPS height on NAVD 88 benchmarks. In: Balmino G., F. Sano (ed), *New Geoids in the World*, International Association of Geodesy, Bulletin d'Information N. 77, IGeS Bulletin N. 4, 13-36.

Milbert, D. G., and D. Schultz, 1993: GEOID (The National Geodetic Survey Geoid Computation Program). Geodetic Services Division, National Geodetic Survey, NOAA, Silver Spring, MD.

- Milbert, D.G., 1991: GEOID90: A high-resolution geoid for the United States. *EOS*, 72(49), 545-554.
- Moritz, H., 1992: Geodetic Reference System 1980. *Bull. Geod.*, 66(2), 187-192.
- Mortiz, H., 1980: *Advanced Physical Geodesy*. Herbert Wichmann Verlag, Karlsruhe, 500 pp.
- Rapp, R.H., 1996: Use of potential coefficient models for geoid undulation determinations using a spherical harmonic representation of the height anomaly/geoid undulation difference. Submitted to *Journal of Geodesy*.
- Rapp, R. H. and R. S. Nerem, 1994: A joint GSFC/DMA project for improving the model of the Earth's gravitational field. Presented at Joint Symposium of the International Gravity Commission and the International Geoid Commission, Graz, Austria, September, 1994.
- Rapp, R.H., 1992: Computation and accuracy of global geoid undulation models. *Proceedings of the Sixth International Geodetic Symposium on Satellite Positioning*, Columbus, Mar. 17-20, 1992. The Ohio State University, pp. 865-872.
- Rapp, R.H., Y.M. Wang, and N.K. Pavlis, 1991: The Ohio State 1991 geopotential and sea surface topography harmonic coefficient models, *Report No. 410*, Department of Geodetic Science and Surveying, The Ohio State University, Columbus, OH. 94 pp.
- Row III, L.W. and M.W. Kozleski, 1991: A microcomputer 30-second point topography database for the conterminous United States, *User Manual, Version 1.0*, National Geophysical Data Center, Boulder, CO, 40 pp.
- Schwarz, K.P., M.G. Sideris, and R. Forsberg, 1990: The use of FFT techniques in physical geodesy. *Geophysical Journal International*, 100, pp. 485-514.
- Sandwell, D. T. and W. H. F. Smith, 1996: Marine Gravity Anomaly from Geosat and ERS-1 Satellite Altimetry, submitted to *J. Geophys. Res.*
- Smith, W.H.F., and P. Wessel, 1990: Gridding with continuous curvature splines in tension. *Geophysics*, 55(3), 293-305.
- Strang Van Hees, G., 1990: Stokes formula using fast Fourier techniques. *Manus. Geod.*, 15(4), 235-239.
- Tscherning, C.C., R.H. Rapp, C. Goad, 1983: A comparison of methods for computing gravimetric quantities from high degree spherical harmonic expansions. *Manuscripta Geodetica*, 8(3), 249-272.
- Zilkoski, D.B., J.H. Richards, and G.M. Young, 1992: Results of the general adjustment of the North American Vertical Datum of 1988. *Surv. and Land Info. Sys.*, 52(3), 133-149.